Nanoscale

Accepted Manuscript

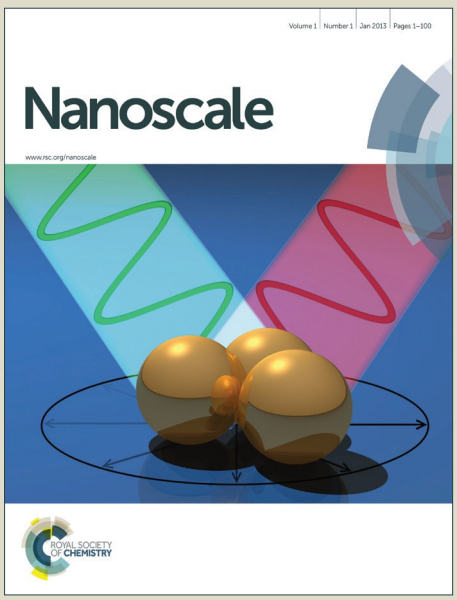

ROYAL SOCIETY OF CHEMISTRY

www.rsc.org/nanoscale

THE INTRINSIC LUMINESCENCE OF INDIVIDUAL PLASMONIC NANOSTRUCTURES IN AQUEOUS SUSPENSION BY PHOTON TIME-OF-FLIGHT SPECTROSCOPY

*Matthieu Loumaigne,[a,f] Julien R. G. Navarro,[b,‡] Stéphane Parola,[b] Martinus H. V. Werts[a] and Anne Débarre[c]**

[a] École normale supérieure de Rennes, CNRS, SATIE (UMR8029), Campus de Ker Lann, F-35170 Bruz, France

[b] École normale supérieure de Lyon, CNRS, Univ. Lyon 1, Laboratoire de Chimie (UMR 5182) F-69364, Lyon, France

[c]Laboratoire Aimé Cotton (UMR 9188), CNRS, Univ. Paris-Sud, F-91405 Orsay, France and PPSM (UMR 8531), CNRS, Institut d'Alembert, École normale supérieure de Cachan, F-94235 Cachan, France.

*: CORRESPONDING AUTHOR Tel: +33-1-47-40-74-43. E-mail: anne.debarre@lac.u-psud.fr.

[f]: present address: MOLTECH Anjou (UMR6200), Univ. Angers, CNRS, F-49045 Angers, France

‡ present address: Arrhenius Laboratory, Department of Materials and Environmental chemistry, Stockholm University, Stockholm, Sweden

Keywords : metal particle luminescence, nanostar, nanobipyramid, fluctuation correlation spectroscopy, light scattering, photon time of flight spectroscopy

Abstract

We have studied the intrinsic one-photon excited luminescence of freely diffusing gold nanoparticles of different shapes in aqueous suspension. Gold nanospheres were used as a reference, since their luminescence has been investigated previously and their light absorption and scattering properties are described analytically by Mie theory. We then studied gold nanobipyramids and nanostars that have recently gained interest as building blocks for new plasmonic nanosensors. The aim of our study is to determine whether the luminescence of gold nanoparticles of complex shape (bipyramids and nanostars) is a plasmon-assisted process, in line with the conclusions of recent spectroscopic studies on spheres and nanorods. Our study has been performed on particles in suspension in order to avoid any artefact from the heterogeneous environment created when particles are deposited on a substrate. We employ a recently developed photon time-of-flight method in combination with correlation spectroscopy of the light scattered by the particles to probe the luminescent properties of individual particles based on a particle-by-particle spectral analysis. Furthermore, we have performed resonant light scattering spectroscopic measurements on the same samples. Our work demonstrates the power of our time-of flight method for uncovering the plasmonic signatures of individual bypramids and nanostars during their brief passage in the focal volume of a confocal set-up. These spectral features of individual particles remain hidden in macroscopic measurements. We find that the intrinsic photoluminescence emission of gold bipyramids and gold nanostars is mediated by their localized surface plasmons.

Introduction

The intrinsic photoluminescence of plasmonic nano-objects provides an interesting alternative to their more commonly used light scattering[1–8] for detecting and studying such particles. The luminescence of noble metals can be observed under one- or multi-photon excitation conditions. The interest for this type of metal-based photoluminescence (PL), initially studied by Mooradian on smooth metallic films,[9] has been renewed since the discovery that metal nanoparticles have a much higher PL quantum yield in comparison to these smooth films.[10] In *ensemble* measurements, PL quantum yields were obtained varying from 10^{-6} to 10^{-4} for gold nanospheres[11] and in the range 10^{-4} to 10^{-3} for gold nanorods,[12] whereas smooth gold films have a quantum yield on the order of 10^{-10}. Very large two-photon absorption cross-sections have been measured for gold nanoclusters.[13] The studies of gold nanoparticle luminescence have been extended to the single particle level, beginning with gold nanospheres under two-photon excitation.[14] Interestingly, Yorulmaz et al. reported that the quantum yield for nanorods with a longitudinal plasmon resonance beyond 650 nm is an order of magnitude larger than that of spherical particles.[15] The growing interest for nanorods may be explained by the fact that these particles sustain a longitudinal surface plasmon whose frequency varies with the aspect ratio of the nanorod.[15,16]

The mechanism behind the photoluminescence of plasmonic nanoparticles is not yet entirely clear. Different processes have been proposed to explain the luminescence mechanism: (1) energy transfer from an electron-hole pair to a surface plasmon and vice versa,[11,16] or (2) a specific electromagnetic antenna effect of the particle.[12] More recently, an electron-hole assisted indirect energy transfer between the transverse and longitudinal plasmon resonances has been suggested in the case of gold nanorods.[17] These models account for the experimental observation that the photoluminescence spectrum for spheres and nanorods correlates well with the light scattering spectrum[15–19] even if some shifts in wavelength have been observed.[15]

In most of the single particle studies, the objects are deposited onto a substrate with which they interact. Deposited particles are immobile and can be illuminated for a substantial amount of time, which enables

the measurement of weak signals and the resolution of the emission spectrum. Substrate-immobilized particles are also suitable for correlating the structural properties of the studied object with its optical response by combining optical spectroscopic and electron microscopic analyses on the same objects. The role of the substrate and the orientation of the nano-object with respect to the substrate nevertheless complicate the analysis. Moreover, the number of studied objects is necessarily limited, which is not favourable for statistical analysis, and sample heterogeneity can hardly be accounted for.

Studies performed on single metallic particles freely diffusing in (aqueous) solution have several advantages. The particles are in a homogeneous, isotropic environment. Moreover, large numbers of individual objects in a given liquid sample can be monitored, without any prior selection bias. Fluctuation correlation spectroscopies (FCS) have already been used to study the dynamics of the luminescence process of gold nanospheres and nanorods diffusing in water.[14,16,18,19] Moreover, combination of photoluminescence FCS (here referred to as PL-FCS for consistency, but generally known as *fluorescence* correlation spectroscopy) with FCS of the light scattering (LS-FCS, sometimes called scattering correlation spectroscopy) provides additional information on the size and shape of the particles. In the case of anisotropic nanoparticles, additional polarization measurements can further help in analyzing the luminescence response. Nevertheless, recording the emission spectrum of single particles diffusing in solution is challenging. It often requires an increase of the observation time for each particle either by using large particles that slowly diffuse through the excitation volume or by increasing the viscosity of the solution.

Recently, we have developed a photon time-of-flight spectroscopic method, named PTOFS, which overcomes this drawback.[20] The principle of the method relies on the transformation of a spectral dispersion into a temporal dispersion using a long optical fiber, which allows us to recover the spectrum of each diffusing particle over a wide range of wavelengths, typically from 400 nm to 1100 nm. This method is closely related to the so-called dispersive Fourier transformation, which has been developed to encode in the time-domain the spectrum of a fast pulse by using the chromatic dispersion of a medium, in order to

perform single-shot measurements. The ability of the method to perform ultrafast real-time spectroscopy has been exploited in different fields, such as the detection of rare events in biology or the discovery of optical rogue waves.[21]

In this work, we combine PL-FCS, LS-FCS and PTOFS to study the intrinsic luminescence of individual plasmonic nanostructures in aqueous suspension. Additionally, *ensemble* measurements of the absorption and scattering properties of the samples in solution have been performed. The nanostructures of interest are gold spheres, gold bipyramids and gold stars. The spheres were included as reference objects for validation of the methodology. Bipyramids and stars have recently attracted a particular interest because they offer the opportunity of high electromagnetic field concentration at their tips.[22–32] The intrinsic luminescence of these nanostructures or their optical properties have not yet been studied experimentally in solution.

After introducing the experimental methodology used, we report on the experimental results obtained on the intrinsic luminescence of gold nanospheres, gold nanobipyramids and gold nanostars. We discuss the new statistical methods that have been applied to PTOFS to extract information on the nanostructures. We describe the luminescence of bipyramids and demonstrate how spectral selection can be a powerful method not only for extracting the intrinsic emission of the nanostructures but also for identifying the presence of an impurity in the solution. We subsequently report on the properties of luminescence of gold nanostars. The complexity of their luminescence spectra is discussed in the light of the models developed to account for the extinction spectrum of deposited nanostars. Our results demonstrate the interest of the combination of a spectral analysis of individual bursts of photons with a pure temporal analysis for the analysis of the intrinsic luminescence of plasmonic structures. Comparison with the ensemble light scattering spectra of the same samples highlights the plasmonic origin of their intrinsic luminescence, which is of great interest for the imaging of these plasmonic nanoparticles in biological media.

Experimental

Materials

Reference gold nanospheres with a diameter of 80 nm in aqueous solution were obtained from BBI International (Cardiff, UK), and used as received. All samples were diluted with air-equilibrated purified water as necessary, in order to obtain samples of sufficiently low optical density (bulk measurements) or sufficiently low particle concentration (fluctuation correlation spectroscopy).

Nanoparticle synthesis

The gold nanostars[22] and gold bipyramids[22,33] were synthesized using a seed-mediated growth process (two-step synthesis). The gold nanoparticles were purified through centrifugation steps (4200x *g*, 20 min.). The supernatant was removed and replaced with milliQ water. This purification step was repeated twice. The gold nanoparticles were functionalized with an anionic polyelectrolyte using the layer-by-layer process as described previously.[23] Briefly, the purified particles were dispersed in 5 mL of milliQ water and an aqueous solution of PSS (30 mg/3mL) was slowly added under constant stirring. The suspensions were finally stirred for 24h and stored in the dark. The bipyramids have a tip-to-tip distance of 110 (+/-16) nm and a base diameter of 37 (+/- 5 nm). The stars have an outer diameter of 130 (+/- 10) nm, and have 10 (+/- 3) tips. TEM images are shown in Figure 1.

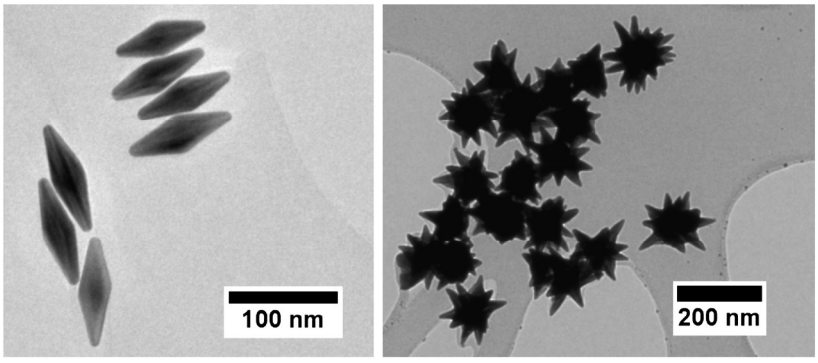

Figure 1. TEM images of gold nanobipyramids (left) and nanostars (right).

Light extinction and scattering measurements on bulk suspensions

Bulk optical spectroscopic measurements were carried out on aqueous suspensions of nanoparticles contained in standard 1 cm plastic or quartz spectroscopic cells. When required, the suspensions were diluted using air-equilibrated purified water. Extinction spectra were measured using a single-beam fiber-coupled CCD spectrometer (USB4000-VIS-NIR, Ocean Optics, USA) and a fiber-coupled tungsten-halogen light source (6.5 W, 3100 K, LS-1, Ocean Optics) equipped with a BG34 color correction filter. The extinction spectra of the three different nanostructures are displayed in Figure 2.

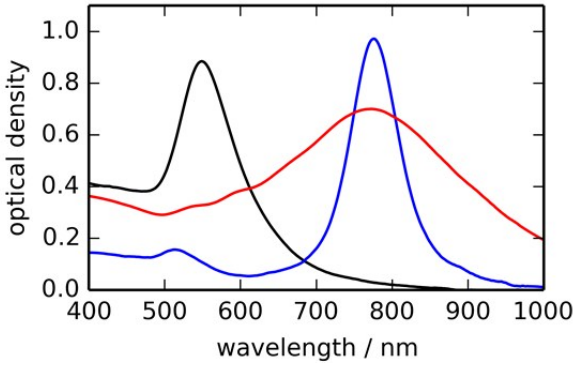

Figure 2. Extinction spectra of 80 nm gold nanospheres in water (black line), gold nanobipyramids in water (blue line) and gold nanostars in water (red line). The optical densities of the suspensions have been arbitrarily scaled for clarity.

Spectra of the resonant light scattering (RLS) of the nanoparticle suspensions were measured in right angle geometry on samples contained in standard 1 cm spectroscopic cells using the methodology that we developed recently,[34] and which is further refined in the present work. The complete procedure is detailed in the Electronic Supplementary Information, and is based on comparing intensities of light scattered by the samples to a reference scatterer. As a reference we used diluted Ludox suspension, which behaves as a perfect Rayleigh scatterer.[35] The method yields scattering spectra whose intensities are proportional to the scattering cross sections $\sigma_{\mathrm{sca}}(\lambda)$. The scattering cross section is related to the extinction cross section $\sigma_{\mathrm{ext}}(\lambda)$ via $\sigma_{\mathrm{sca}}(\lambda) = \varphi_{\mathrm{LS}}(\lambda)\sigma_{\mathrm{ext}}(\lambda)$, where φ_{LS} is the (wavelength-dependent) scattering efficiency.

Single particle optical measurements

In a typical photon time-of-flight spectroscopy (PTOFS) experiment[20] the sample is illuminated by a pulsed light source, in our case a frequency-doubled titanium-sapphire laser (repetition rate 80 MHz, pulse width 100 fs, Figure 3, #1). The light signal generated by the particle diffusing through the excitation volume is divided over two detection paths by a beam splitter (Figure 3, #2). In the first path (Figure 3, #3), the photons are directly detected by an avalanche photodiode. This path allows detecting either elastically scattered light or luminescence, depending on the choice of the optical filters that are inserted in the optical path. The signal from this path can be used for generating fluctuation correlation spectroscopic (FCS) profiles, and for identification of bursts indicating the presence of an active object in the focal volume.

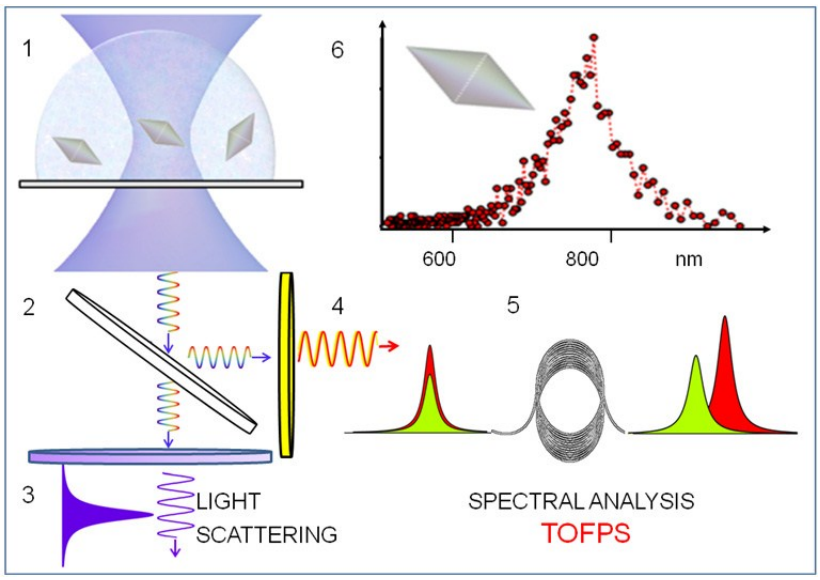

Figure3. Principle of the experimental procedure. 1-Confocal volume illuminated by a pulsed excitation; 2-Chromatic splitting of the collected emission; 3-Single-photon detection of elastically scattered photons; 4-Selection of luminescence photons using an optical filter; 5-Spectral dispersion of the luminescence photons after coupling into a long optical fiber; 6-Example of luminescence spectrum of a single nanobipyramid.

In the second path (Figure3, #4), the photons are sent into a dispersive medium (94 meter long optical fiber, Figure 3, #5), which is connected to a second avalanche photodiode. As a result, the initial burst of light emitted during the passage of the luminescent object in the focal volume is temporally dispersed and its spectrum is encoded in the temporal profile of the burst at the exit of the fiber. This temporal profile is measured using the APD and the time-correlated photon counting electronics. While in the focal volume, the object undergoes many excitation-deexcitation cycles, a histogram of the time delay between excitation and emission events is built up using time-correlated single photon counting techniques. This effectively yields the time-of-flight spectrum of the photons emitted from the focal volume as a result of the exciting short laser pulse (Figure 3, #5 & 6). The experimental and burst selection procedures are detailed in the Electronic Supplementary Information (S1-2, ESI).

Results and Discussion

Spectral analysis of single bursts of luminescence from individual nano-objects in solution is a challenge in single particle spectroscopy, because of the limited time that a diffusing small particle spends in the excitation volume. Replacing spatial dispersion of light using prisms or gratings with temporal dispersion using a glass fiber offers a valuable opportunity to overcome this limitation, which is the principle of the photon time-of-flight spectroscopy (PTOFS).[20] The major advantage of this method is the replacement of a multichannel detector by a single-channel detector, which can efficiently enhance the temporal resolution and additionally reduce the cost and complexity of the set-up. The PTOFS method is capable of recording the full emission spectrum of a single object diffusing through the focal volume in only a few milliseconds. Beyond the spectral analysis of individual bursts of luminescence, PTOFS can be combined with other time-correlated spectroscopic signals, for example with elastic light scattering or luminescence.

In the present work, the studied luminescence emission is very short-lived, decaying much faster than the temporal response of our set-up (which is ~250 ps FWHM). This observation is consistent with the reported lifetime of the luminescence process around 100fs.[36] PTOFS is particularly appropriate to the analysis of this type of signal. Indeed, the measured delay (in the ns domain) between the excitation pulse and the arrival time of the photon emitted by the corresponding nanoparticle is only due to the chromatic dispersion inside the optical fiber. We have developed an algorithm that allows retrieving the emission spectrum over a desired time range. This time interval can span many individual bursts (*i.e.* the passing of several objects in the focal volume) or be as short to span only parts of a single burst (*i.e.* a spectral snap-shot of a single object at a specific instant during its passage). In the first situation, the spectrum obtained on a sufficiently large number of bursts can be compared to the spectrum acquired in a macroscopic *ensemble* experiment. The second case provides details on the dynamics of the emission of a single particle.

Luminescence and light scattering of gold nanospheres freely diffusing in water

In order to validate our methods we have first studied the luminescence of gold nanospheres in aqueous suspension under pulsed excitation at 430 nm. This wavelength is sufficiently apart from the plasmon resonance to be able to filter out the Raman signature of water using optical filters. The choice of wavelength is also guided by the possibility of efficiently separating the elastic light scattering by the particles from their luminescence.

Figure 4 displays the profile of the bulk luminescence spectrum of the gold nanospheres in water whose emission has been averaged over many excitation-deexcitation cycles and many bursts (blue curve). The spectrum of the overall *ensemble* luminescence has a maximum at 560 nm, and has a close spectral similarity with the experimental resonant light scattering (RLS) spectrum of a bulk sample in a spectroscopic cell (also shown in Figure 4, red curve). The similarity between the luminescence spectrum and the RLS spectrum of spheres has been already pointed out in several previous studies. This similarity suggests that the observed intrinsic luminescence of gold nanoparticles is plasmon-assisted.[11,12,16,17,19]

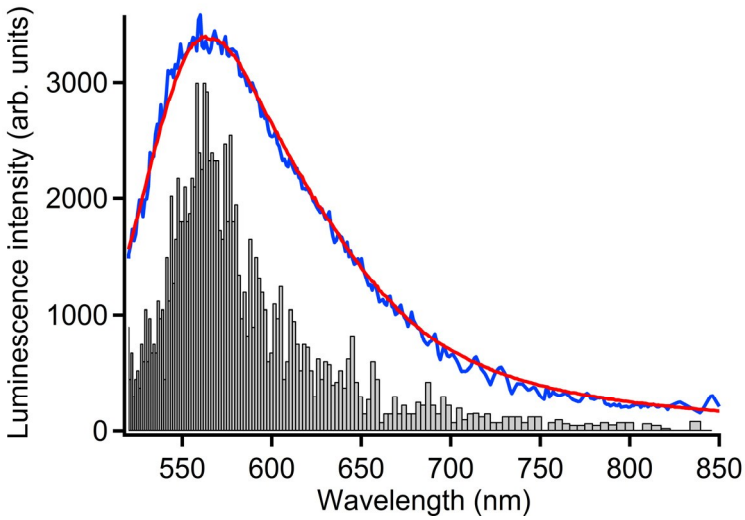

Figure 4. Luminescence and resonant light scattering of 80 nm gold spheres in water. Bulk resonant light scattering (RLS) spectrum recorded using a standard 1 cm spectroscopic cell using white light illumination(red line), bulk one-photon excited luminescence spectrum from PTOFS (excitation wavelength = 430 nm, blue line) and histogram of the peak wavelengths of luminescence of individual particles (gray bars) obtained by analyzing the TOF spectra of individual bursts.

An example of a luminescence spectrum emitted by a single sphere during its passage through the focal volume is shown in Figure 5b. This spectrum was extracted from a single burst in a sequence of many bursts as depicted by the time histogram (Figure 5a).

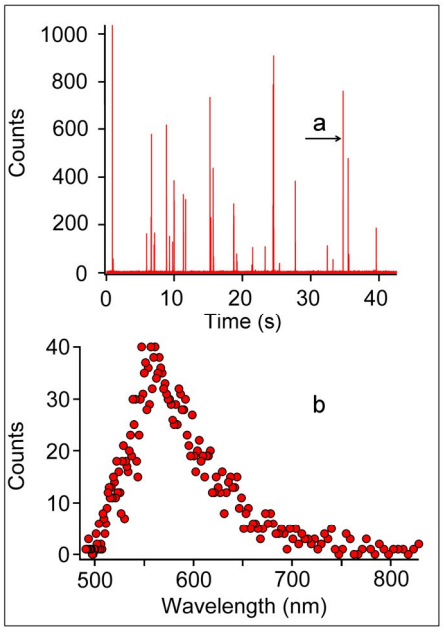

Figure 5. Luminescence of 80 nm gold spheres. Top: example of bursts in the time histogram; Bottom: example of luminescence spectrum of a single sphere corresponding to the burst indicated by the arrow in Figure 4a (excitation wavelength 430 nm, P=1400 μW).

One of the advantages of our PTOFS method is the flexibility of the numerical post-processing procedures that can be developed to exploit the large amount of information contained in the simultaneous recording of the absolute arrival time ("macrotime") and of the wavelength for each emitted photon (delay relative to the excitation pulse, encoded in the "microtime"). Each burst corresponding to a passing particle is described by its PTOF spectrum. This offers for example the opportunity of constructing a histogram of peak emission wavelengths of the luminescence spectrum of the individual bursts. Here, we demonstrate the principle of this novel procedure by applying it to the PTOFS recordings of the nanosphere model system.

The first step of the procedure involves the identification of all individual bursts in the time histogram, as explained in the Electronic Supplementary Information (S1-2). Each burst corresponds to the emission of light by a particle that crosses the excitation volume. In a second step, the PTOF spectrum is extracted from the data for each burst and the wavelength of the maximum of this spectrum is identified. The

corresponding distribution of maxima yields the histogram of the bursts with respect to the peak wavelengths of the spectra of the bursts. An example of such a histogram is displayed in Figure 4. The full width at half maximum (FWHM) of the histogram is about 35 nm, a width which reflects the distribution of the sizes of the gold nanospheres diffusing in water. The width of the *ensemble* luminescence spectrum, of the order of 110 nm, thus corresponds roughly to the convolution of this distribution with the width (~90 nm) of the plasmon resonance of a gold nanosphere of 80nm diameter. The information included in the histogram and in the time-integrated PTOFS luminescence spectrum is complementary. The histogram provides a measure of the number of particles that emit with a given peak wavelength whereas the time-integrated luminescence spectrum gives the intensity of the signal with respect to wavelength. The comparison between both data provides information on the luminescence efficiency of the objects.

Finally, the autocorrelation of the Rayleigh scattering allowed measuring the size and the concentration of the particles. The autocorrelation of the Rayleigh scattering (Electronic Supplementary Information, Figure S4) corresponds to the Brownian motion of spheres with a hydrodynamic radius of 83 nm.

Correlated analysis of the photoluminescence and light scattering of gold bipyramids in water

Until now, the only anisotropic nanoparticles of well-defined geometry whose one-photon excited luminescence has been studied are gold nanorods. The similarity between the shapes of the luminescence and the scattering spectra has been demonstrated for single nanorods with different aspect ratios deposited on a substrate.[15,16] In the following, we extend the measurement of one-photon excited luminescence of plasmonic structures to the case of gold bipyramids in aqueous suspension. Bipyramids are attractive nano-objects since their shape symmetry leads to the existence of two orthogonal plasmon modes. Similarly to nanorods, the frequency of the longitudinal plasmon resonance can be tuned by adjusting the ratio between the dimensions of the basis and height of the pyramid. However, in contrast to gold nanorods, the bipyramids have sharp tips at their extremities, where the confinement of the electromagnetic field can be even more efficient. Bipyramids combine the plasmonic sensing capabilities of

elongated plasmonic particles with an increased efficiency for SERS.[25] Their light scattering has been studied on individual particles deposited on a substrate in combination with numerical modeling based on structural parameters deduced from TEM measurements including the tip shape,[26] but no measurement of their intrinsic luminescence has been made.

In the present study, the sample of bipyramids has been excited at 430 nm, under similar conditions as those used above for the 80 nm gold spheres. Our analysis starts with the autocorrelation profile of the elastic light scattering (LS-FCS) of the bipyramids, displayed in Figure 6 .

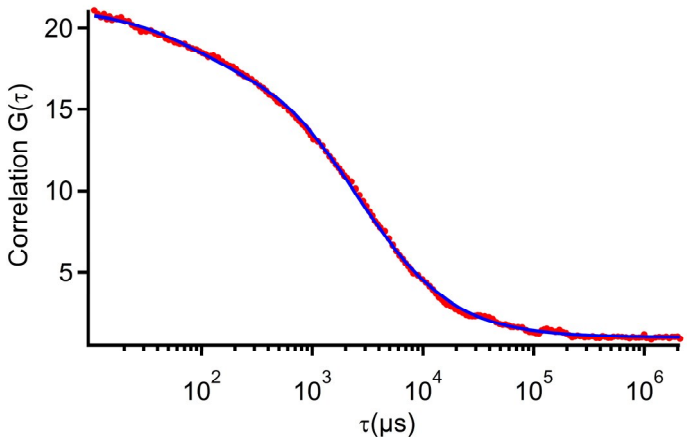

Figure 6. Correlation profile of the elastic light scattering by gold bipyramids (λ = 430 nm). Red dots, experimental curve; Blue line, fit according to Equation 5.

The LS-FCS autocorrelation profile of the bipyramids is best described by the product of the correlation function of Brownian diffusion $G_D(\tau)$ and a rotational term (Equation 5).

$$G(\tau) = 1 + G_D(\tau)\left(1 + Ce^{-\tau/\tau_r}\right) \quad (5)$$

$$G_D(\tau) = \frac{1}{2\sqrt{2}N} \frac{1}{\left(1+\frac{\tau}{\tau_D}\right)\sqrt{1+\left(\frac{\omega_r}{\omega_z}\right)^2 \frac{\tau}{\tau_D}}} \quad (6)$$

In this expression, τ_D is the diffusion time. N, ω_r and ω_z are the mean number of particles simultaneously present in the excitation volume, and the radial and axial waists of the excitation volume, assuming a 3D Gaussian excitation beam, respectively. τ_r is the rotational time and C is the contrast of the rotational

contribution to the profile.[14] A satisfying fit of the translational contribution was obtained by using a single diffusion time of 2500µs, which is a strong indication that the size distribution of the bipyramids is quite narrow. This corroborates the analysis by TEM.

A rotational time constant of 70 +/- 5 µs was obtained by fitting Eq. 5 to the data. The contrast of rotation C is found equal to 0.15, which is large enough to have a good estimation of the rotation time. Tirado *et al.* have developed a model to account for the diffusion constants for translation and rotation of short nanorods.[37] The order of magnitude of the length *L* of the bipyramids from TEM measurements is 110 nm (± 16 nm). The aspect ratio L/d of nanorods whose time of diffusion would match that of bipyramids of length 110 nm is 1.2. The rotation time of such a nanorod is of the order of 260 µs, larger than that observed for the bipyramids. The rotation time may therefore be used to distinguish a bipyramid from a nanorod.

On the basis of our previous work on the effect of a pulsed excitation on the luminescence of gold nanoparticle excited at one-photon,[18] we can say that the laser induced heating of a 50 nm spherical nanoparticle immersed in water does not have a significant impact on its hydrodynamic radius. The volume of the bipyramids is comparable with the volume of a 50 nm diameter sphere. Since the absorption cross section associated to the intraband transitions (far from the plasmonic resonance) is mainly governed by the volume of the nanoparticle and not its shape, we can draw the same conclusion for the bipyramids.

The LS-FCS autocorrelation curve gives access to the concentration of particles in the sample *via* its amplitude $G_D(0)$ at zero time lag (Equation 6), since this amplitude is inversely proportional to the number of particles *N* present on average in the focal volume. The determination of the concentration using this amplitude relies on calibration of the focal volume,[38] which was achieved using samples of known concentration and optical response (Rhodamine 6G in water and 50 nm gold nanospheres in water). Based on the concentration of the samples from FCS, and the bulk UV-visible extinction spectra of the same sample, the extinction cross-section of the nanobipyramids at any wavelength can be estimated. Three independent measurements were done and this yields an extinction cross-section of the gold

nanobipyramids in water of 2.4 (± 1.6) x 10^{-10} cm^2 at the maximum of the plasmon band at 772 nm. A value of 1.5 10^{-10} cm^2 was reported in reference 26 for a gold bipyramid of nearly same aspect ratio but a shorter length of 77 nm.

For comparison, we have furthermore estimated the maximum extinction cross-section of a (theoretical) nanorod in water with a diameter of 37 nm and an aspect ratio of 3, matching the longitudinal and transverse dimensions of the bipyramids. The nanorod was given the shape of a spherically capped cylinder and the geometrical factors tabulated by Prescott and Mulvaney were used.[39] The calculated value of the extinction cross-section of this nanorod model, ~6 10^{-10} cm^2 is on the same order of magnitude as the experimental value measured here for bipyramids which are of same dimensions but smaller volume.

A typical example of the raw luminescence spectrum of an *ensemble* of gold bipyramids in water acquired by PTOFS averaged over the entire acquisition time (56 seconds) is displayed in Figure 7a. In this spectrum, a clear emission band appears at long wavelengths (λ_{max} ≈772 nm). Additionally, a shoulder is observed at shorter wavelengths (between approximately 500 and 650 nm). However, this short-wavelength shoulder is not observed in the spectrum of individual bursts (Figure 9), which indicates that it is not an intrinsic feature of the gold bipyramid luminescence. In the Electronic Supplementary Information (S1-3), we demonstrate how we isolate, identify and eliminate this spurious contribution, which is due to a fluorescent molecular impurity, to the overall luminescence spectrum, using a burst-selection procedure on the individual bursts, obtaining a luminescence spectrum of 'pure' gold bipyramids (Figure 7b). It can be seen as another demonstration of the versatility of the PTOFS method.

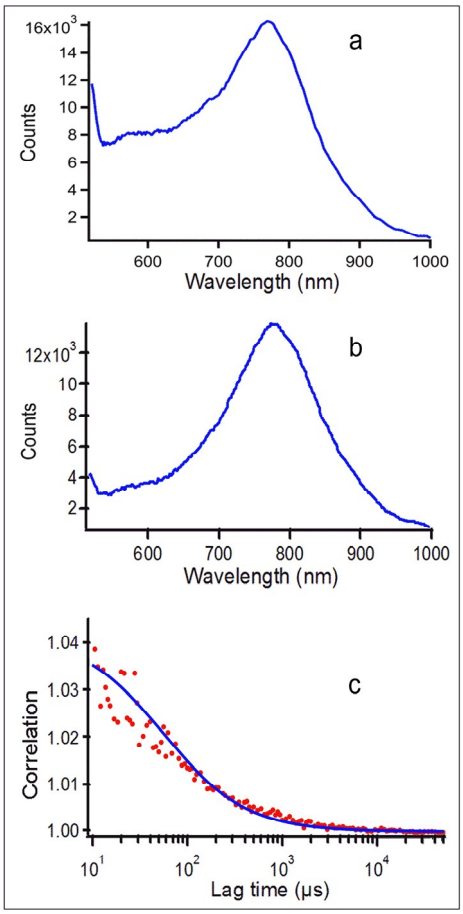

Figure 7.*Ensemble*-averaged spectrum of luminescence of gold bipyramids in water. (a) spectrum deduced from the raw histogram of photons; (b) spectrum rebuilt after burst filtering procedure (see ESI, S1-3); (c) correlation function of the residual signal.

After filtering out the contribution of the fluorescent impurity using the burst selection procedure, we have built the histogram of the bursts of luminescence with respect to their wavelength maximum, as we have done previously for the gold nanospheres. Figure 8 superimposes this histogram, the filtered luminescence spectrum, and the light scattering spectrum.

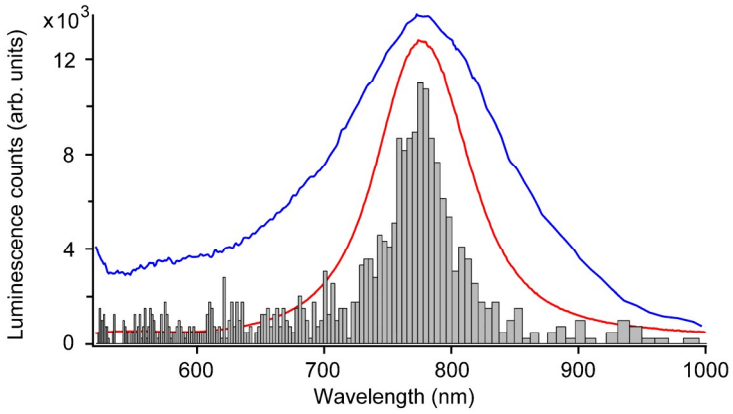

Figure 8. Spectral properties of the luminescence of gold bipyramids freely diffusing in water. Blue curve: luminescence spectrum acquired by PTOFS, after filtering by burst selection. Grey bars: histogram of the maximum wavelength of the spectra of individual bursts. Red curve: experimental ensemble light scattering spectrum of the bipyramids.

The maxima of the luminescence and of the RLS spectra coincide fairly well. Moreover, the luminescence spectrum clearly overlaps with the scattering spectrum. These observations suggest that the one-photon excited luminescence of bipyramids is a plasmon-assisted process, as previously determined for nanorods,[15–17,36] and nanospheres.[11,15,16,36] Our observations on gold bipyramids thus extend the results of previous studies on gold nanoparticle luminescence to an object with a more complex shape.

However, we also note that in the case of bipyramids, contrary to the case of gold nanospheres, the profile of the total luminescence spectrum is broader (FWHM~160 nm) than the spectrum of the scattering process (FWHM~85 nm). Theoretical calculations have demonstrated that the width of the scattering spectrum of a single bipyramid itself is larger than the width of the corresponding spheroid with similar resonance frequency.[24] The broadening of the plasmon resonance of bipyramids has been recently studied in detail.[26] The possible role of chemical interface damping, induced by the presence of molecules at the surface of the particles, was pointed out. The role of the molecules at the interface between a nanoparticle surface and water has also been evoked in the case of luminescence of spherical particles.[14] We propose therefore that chemical damping is likely to play a role in the broadening of luminescence of bipyramids in

water. Whereas the width of the histogram of peak maxima is narrow (FWHM∼40 nm), which corresponds to a narrow distribution of shapes of the synthesized bipyramids, we note the presence of objects whose wavelength peak is shifted towards the blue range (from ∼520 nm to ∼700 nm), indicating the presence of bipyramids of smaller aspect ratio or more spherical objects. It can explain the slight asymmetry in the profile of the luminescence spectrum. The profile of the scattering spectrum, however, is nearly symmetrical. This difference could be explained by the fact that the scattering emission efficiency depends strongly on the size of the particle (*e.g.* for spheres as the sixth power of the diameter) whereas the dependence of the luminescence intensity on the size of the particles is not straightforward. Consequently, the contribution of smaller particles to the overall intensity at a given wavelength can be different for both processes.

In order to further investigate the effect of particle size and shape heterogeneity on the width of the overall luminescence spectrum, it is useful to extract the luminescence spectra of individual bursts due to the passage of a bipyramid through the focal volume. Some typical luminescence spectra of single bipyramids are displayed in Figure 9.The large majority of the bipyramid luminescence spectra have a width of the order of 75 to 110 nm, as illustrated by spectra 1, 2 and 4. The narrowest spectrum (Figure 9- 4) has a profile that can be described fairly well by a Lorentzian shape of 75 nm FWHM, for example.

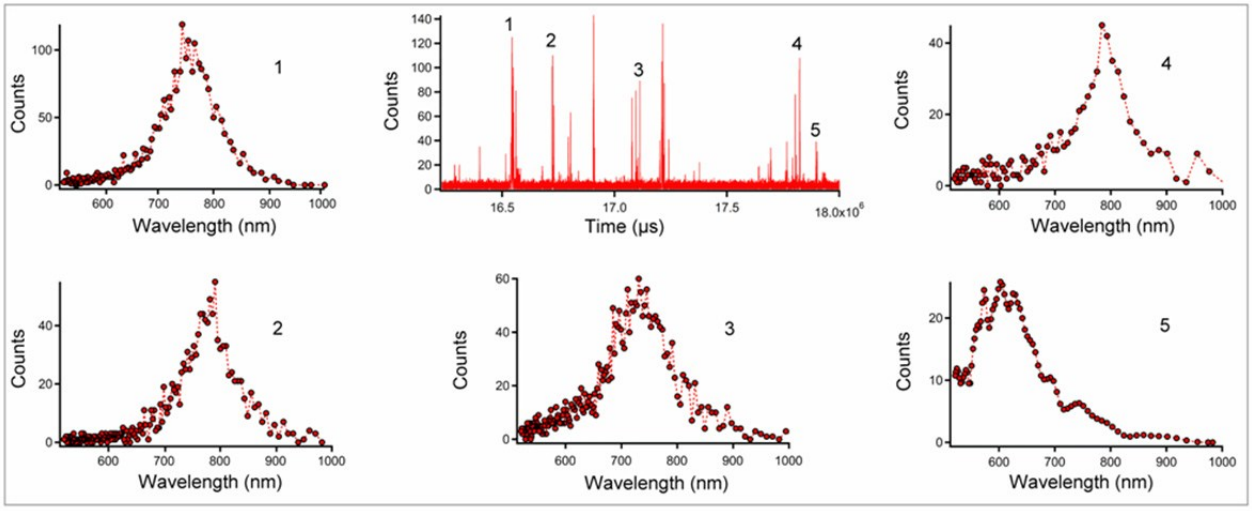

Figure 9. Luminescence spectra of individual bipyramids, numbered 1 to 5 on the corresponding time trace of luminescence intensity.

A limited number of bipyramids show a broader spectrum, such as the bipyramid of spectrum 3, whose width is 120 nm (Figure 9-3). A broadening of the luminescence spectrum with respect to the scattering spectrum has also been noticed in the case of single deposited nanorods, which is more pronounced for low aspect ratio objects.[15] The last example of Figure 9 (spectrum 5) corresponds to a more spherical object, which contributes to the blue wing of the total luminescence spectrum. We have applied an automated procedure to describe the shape of the bipyramid PL to a series of a large number of PTOFS luminescence spectra recorded on diffusing, individual bipyramids, and recorded the widths (full widths at half maximum, FWHM) in a histogram (see Supporting Info, Figure S7). This histogram shows a monomodal distribution centered around a typical spectral width of65 nm. The standard deviation is 25 nm. The origin of the broadening of the overall luminescence spectrum compared to the RL scattering spectrum can only partly be explained by the presence of particles with a blue-shifted resonance and by that of broad spectra objects. The origin of the discrepancy between both spectra deserves additional investigations.

To summarize, the PTOFS measurements combined with RLS spectroscopy on the same sample of bipyramids has allowed demonstrating that also in the case of gold bipyramids the RLS and luminescence

spectra overlap and that their maxima are in coincidence. This extends prior observations[11,15–17,36] on plasmonic nanospheres and nanorods. It suggests that the intrinsic one-photon excited luminescence is a plasmon assisted process. However, the broad width of the luminescence spectrum cannot be readily explained by this model. The very good signal-to-noise ratio obtained in the detection of single bipyramids allows for the measurement the luminescence spectrum of single, individual bipyramids, even in the presence of a fluorescent impurities as in the present case.

Light scattering and intrinsic photoluminescence of gold nanostars in water

The interest of using bipyramids instead of nanorods is the presence of sharp tips at their extremities, which enables large local enhancements of the electromagnetic field. From this point of view, nanostars appear to be even more promising. With the growing complexity in shape of nanostars comes the difficulty to model their optical response. A hybridization model has been successfully combined with FDTD calculations to reproduce the experimentally measured scattering spectra and to interpret the main plasmon resonances in the case of a deposited nanostar.[28,31] The calculations demonstrate that the scattering spectrum of a gold nanostar presents different resonances, which depend on the number of tips and on their lengths and their radii of curvature. The spectral position of these resonances spreads over a large range. Consequently, the scattering spectrum of an individual gold nanostar is broad and shows a structure composed of overlapping resonances, in contrast to gold bipyramids whose spectra are narrow and mainly consists of the band of the longitudinal resonance. The width and the structure of the optical spectrum of a nanostar both depend on the shape of the nanostar, which is unique for each specimen.

The time-correlation profile of the light scattering intensity of the gold nanostar sample (LS-FCS) presents a diffusion contribution with a characteristic time τ_D of 2450 µs, which corresponds to a particle with a hydrodynamic radius of about 110 nm (Figure S5, Electronic Supplementary Information). There is also a rotational contribution with a weak contrast of 0.07 and a characteristic time of 80 +/- 15 µs, indicating the presence of non-spherical particles, which is compatible with structures of nanostars.

The total luminescence spectrum accumulated over the whole acquisition time presents a bump in the visible range similar to what was observed for the bipyramids. This contribution corresponds to the fluorescence of the same impurity as found in the bipyramid samples and can be numerically filtered out by the burst selection procedure described above. The resulting filtered spectrum is displayed in Figure 10.

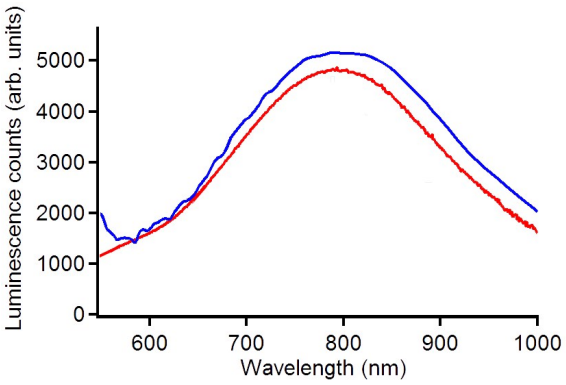

Figure 10. Intrinsic photoluminescence of gold nanostars in water and comparison with resonant light scattering.Blue curve: luminescence spectrum acquired by PTOFS (excitation wavelength 430 nm; P = 1400 µW, filtered using burst selection by intensity threshold). Red curve: experimental ensemble elastic scattering spectrum of the nanostars.

The bulk luminescence spectrum of the nanostars is clearly broader (FWHM~300 nm) than that of the bipyramids (FWHM~160 nm). This profile is in agreement with the spectral profile of resonant light scattering, which displays a similar broad band with a width of nearly 300 nm (Figure 1 and Figure S6 in Electronic Supporting Information).

Interestingly, the high luminescence intensity allows us to follow via PTOFS the time evolution of the emission spectrum of individual particles during their passage through the excitation volume. In fact, the concentration of particles in this sample is quite low, which is confirmed by the high value of $G_D(0)$ (Figure S5, Electronic Supplementary Information). Consequently, the selection of a given burst of luminescence in the intensity *versus* time histogram is unambiguous. Some examples of spectra of freely diffusing nanostars

in water are shown in Figure 11.The spectral analysis of individual bursts reveals that the luminescence spectra of individual nanostars show a large variation between the particles, in contrast to the case of bipyramids.

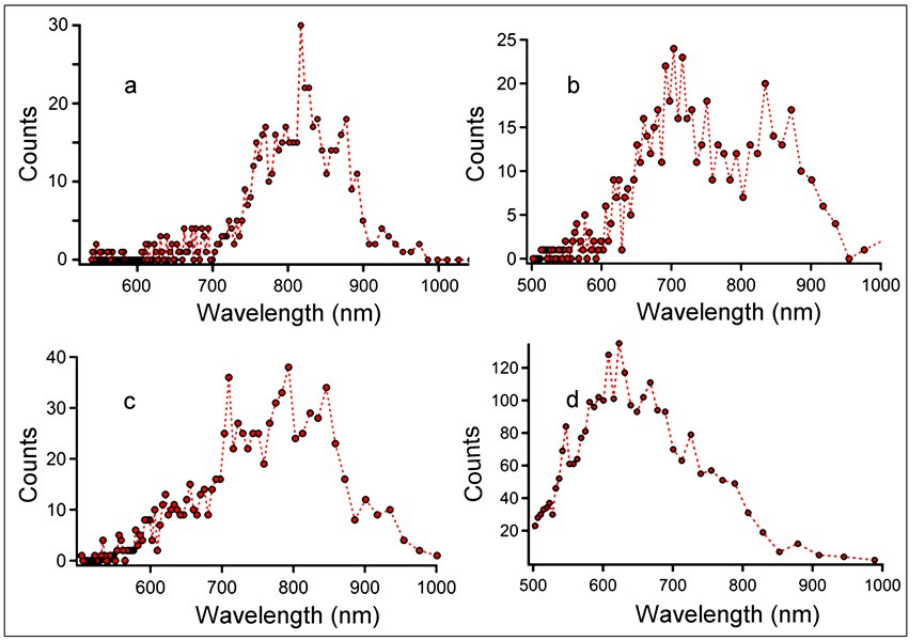

Figure 11. Typical luminescence spectra of single gold nanostars freely diffusing in water; excitation wavelength 430 nm; P = 1400 µW. The spectra were extracted from bursts taken from a 200s long recording.

The most striking spectral features shared by a significant fraction of the luminescent nanostars are a broad width (of the order of 200 nm to 300 nm depending on the spectra) and a profile that displays intensity fluctuations much larger than the inherent statistical fluctuations of the measurement (of the order of $\sqrt{N}$ with N the counts number), assuming a Poisson noise. Consequently, the luminescence spectrum of a given nanostar has not a smooth profile but rather display several peaks on a background.

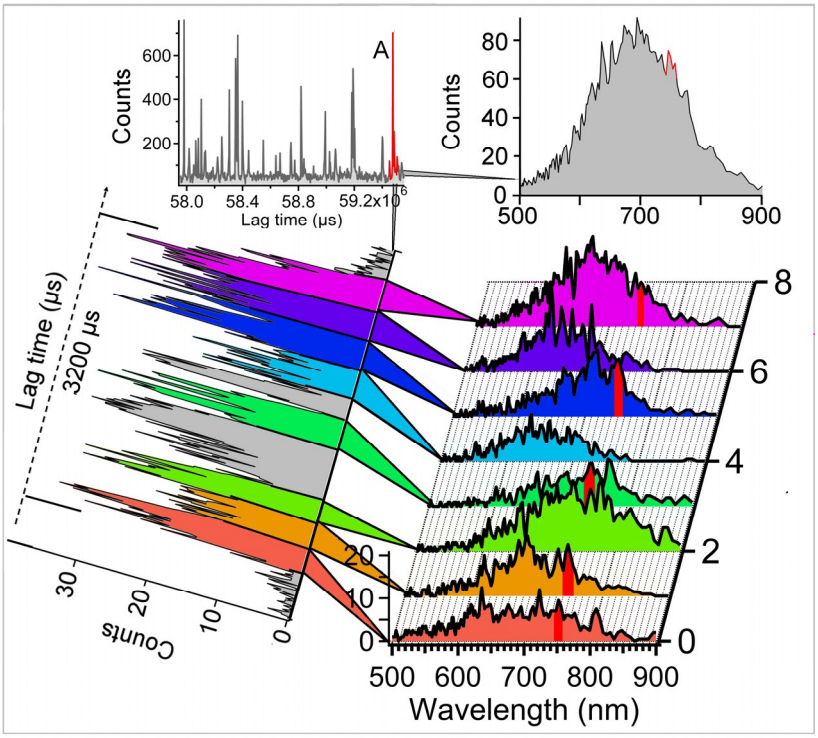

Figure 12. Dynamics of the luminescence of an individual gold nanostar in water crossing the excitation volume. The duration of the passage is 3.2 ms. At the top, on the left side, a fragment of the intensity-versus-time histogram. The burst labeled "A" was analyzed. At the top, on the right side, the total spectrum of the burst (*i.e.* the PTOFS signal accumulated over the total duration of the burst). At the bottom on the left side, a zoom of the burst showing the intensity fluctuations of the count number with respect to time; At the bottom, on the right side the PTOFS luminescence spectra corresponding to the sub-bursts delimited by the lines in the burst structure and by arrows of same colors than the corresponding spectra. In red is schematically underlined the peak at 750nm in the successive spectra.

Additionally, an example of the spectral dynamics of a freely diffusing nanostar in water is shown in Figure 12.The burst analyzed in Figure 12 has duration of 3.2 milliseconds and the width of the corresponding luminescence spectrum is 200 nm. During the burst, the luminescence intensity fluctuates, alternating intervals of high emission intensity separated by intervals where the signal is rapidly fluctuating between different levels. We have divided the burst into 10 intervals separated by the instants that a drop

in emission intensity occurs. From eight of these sub-bursts (for sake of clarity) we derived the luminescence spectrum by PTOFS (i.e. each of the spectra represents a snapshot of approximately 300 µs). This analysis reveals spectral jumps in the emission. Moreover, several peaks are present that are recurrent in different spectra, at varying intensity. This is the case of the peak at ~750nm, for example, which is present on spectra #0, #1, #3, #5 and weakly in #8. The intensity of the peaks in spectra #1, #3, #5 is higher than the amplitude of the noise. It has to be noted that the evolution shown in Figure 12, does not demonstrate a reshaping process, which would have implied a continuous shift of the plasmon resonances towards the blue range. Previous studies have demonstrated that light scattering spectra of deposited gold nanostars present several peaks, whose amplitude and occurrence vary with the polarisation of the excitation light.[28,31] These maxima have been satisfyingly interpreted as the plasmonic resonances resulting from the hybridization of the plasmonic resonances of the core and of the various tips of the nanostar.[31] This plasmonic hybridization is an analogy to the hybridization of electronic wavefunctions, and within this model, the signature of the tips is dominant in the low-energy bonding modes. Depending on the relative orientation of the nanostar and of the polarization of the excitation beam, the amplitude of the different resonances varies, which leads to modifications in the profile of the scattering spectrum.

In this work, spectra of the intrinsic luminescence were acquired under linearly polarized excitation. While passing the excitation volume, the nanostar rotates under Brownian motion and the angle between the light polarization and the axis of each tip of the nanostar varies. The observation of peaks in the structure of the luminescence spectrum in combination with the fluctuations in the luminescence spectrum during the bursts is a strong argument to attribute the observed peaks to the signature of the tips of the given nanostar. This interpretation further strengthens the idea that the luminescence spectrum of a gold nanostar is plasmon-mediated as it is the case for other plasmonic nanoparticles such as the bipyramids studied in this paper, and for nanorods[15–17,36] and nanospheres.[11,15,16,36] The comparison between the resonant light scattering spectrum and the average luminescence spectrum of many nanostars supports this hypothesis (Figure 10).

In the case of bipyramids, the spectra of the single objects are composed of a single peak, which can be attributed to the longitudinal plasmon of the bipyramid. The quite narrow distribution of shapes of the bipyramids in the sample makes the interpretation unambiguous. In contrast, the structure and in particular the number of tips of the nanostars can vary from star to star in the same sample, leading to a change in the corresponding spectral profiles of luminescence. As the nanostar rotates during its passage through the excitation volume (with a rotation time given by FCS of the order of 80µs), the peaks of the spectrum corresponding to the different plasmon resonances are partly washed out over the (sub-)burst duration (with a characteristic diffusion time given by FCS of the order of 2500µs). The spectrum presents clearly distinguishable peaks only in the case of a nanostar of a limited number of tips, such as the spectrum in Figure 11a for which two low energy peaks at 830 nm and 880 nm reveal the presence of two well-defined tips.

Finally, using concentration data from LS-FCS and the *ensemble* UV-visible extinction spectrum as explained above, we have determined an average value of 3.9 (+/- 2.3) x 10^{-11} cm^2 at 793 nm for the extinction cross-section of these nanostars, one order of magnitude lower than that of the bipyramids.

Conclusion

By studying three different types of gold nanoparticles freely diffusing in aqueous suspension, we found that the correlation between the spectra of the intrinsic photoluminescence and the resonant light scattering is also observed for gold bipyramids and gold nanostars. This further strengthens the notion that the intrinsic photoluminescence of gold nanoparticles in general stems from a plasmon-mediated process, independently of the shape of the particle. This study has further highlighted the potential of photon time-of-flight spectroscopy to derive spectral information on the light emission of individual particles in liquid suspension from an analysis of luminescence bursts. In particular, it offers the opportunity to efficiently separate emissions of different spectral characteristics, such as that of a fluorescent impurity and

luminescent gold nanoparticles. It also gives spectroscopic access to the sub-millisecond dynamics of individual nanoparticles as they evolve in the excitation volume.

The basic principle of PTOFS, which resembles that of the dispersive Fourier transform,[21] makes its combination with photon-counting correlation spectroscopies straightforward. In the present study on gold nanobipyramids and nanostars we have combined light-scattering fluctuation correlation spectroscopy (LS-FCS) and PTOFS, which provides simultaneously information about the hydrodynamic radii of the particles and their spectra. Finally, this method proved to be efficient to record spectral fluctuations in the luminescence of individual nanostars rotating in the observation volume under linearly polarized excitation. The presence of multiple peaks in the spectrum of nanostars compared to the simple profile of the spectrum of nanobipyramids can be interpreted as the signatures of the plasmon resonances of the different tips of the nanostars.

Here, we combined PTOFS and fluctuation correlation spectroscopies for the investigation of the intrinsic photoluminescence of plasmonic nano-objects freely diffusing in an isotropic and homogeneous dielectric environment. We obtained information on the single-object level that is complementary to studies on objects deposited on a solid substrate where the environment is inherently anisotropic. Our methodology exploits the single-object detection capability of a confocal detection scheme with the statistical power of correlation analysis and the spectral resolution of photon time-of-flight spectroscopy.

ACKNOWLEDGMENT This work is supported by a public grant overseen by the French National Research Agency (ANR) as part of the “Investissements d’Avenir” program (Labex NanoSaclay, reference: ANR-10-LABX-0035), and by an ANR JCJC 2010 grant (project COMONSENS). JN and SP acknowledge support from French National Research Agency (ANR) P3N project nanoPDT # ANR-09-NANO-027-04.

ELECTRONIC SUPPLEMENTARY INFORMATION AVAILABLE: Additional experimental details, TEM images of gold bipyramids and nanostars, FCS data for spheres and stars, resonant light scattering for gold stars and gold bipyramids, histogram of the widths of the luminescence spectra of individual bipyramids

REFERENCES

1. G. Mie, *Ann. Phys.*, 1908, **330**, 377–445.

2. T. Mappes, N. Jahr, A. Csaki, N. Vogler, J. Popp, and W. Fritzsche, *Angew. Chem. Int. Ed. Engl.*, 2012, **51**, 11208–12.

3. M. Quinten, *Beyond Mie's Theory II – The Generalized Mie Theory, in Optical Properties of Nanoparticle Systems: Mie and beyond,* Wiley-VCH Verlag GmbH & Co. KGaA, Weinheim, Germany, 2011.

4. J. Lin, S. Wang, P. Huang, Z. Wang, S. Chen, G. Niu, W. Li, J. He, D. Cui, G. Lu, X. Chen, and Z. Nie, *ACS Nano*, 2013, **7**, 5320–9.

5. N. Fairbairn, A. Christofidou, A. G. Kanaras, T. A. Newman, and O. L. Muskens, *Phys. Chem. Chem. Phys.*, 2013, **15**, 4163–8.

6. J. Wirth, F. Garwe, J. Bergmann, W. Paa, A. Csaki, O. Stranik, and W. Fritzsche, *Nano Lett.*, 2014, **14**, 570–7.

7. M. Hu, C. Novo, A. Funston, H. Wang, H. Staleva, S. Zou, P. Mulvaney, Y. Xia, and G. V Hartland, *J. Mater. Chem.*, 2008, **18**, 1949–1960.

8. M. A. Mahmoud, D. O'Neil, and M. A. El-Sayed, *Chem. Mater.*, 2014, **26**, 44–58.

9. A. Mooradian, *Phys. Rev. Lett.*, 1969, **22**, 185–187.

10. J. P. Wilcoxon, J. E. Martin, F. Parsapour, B. Wiedenman, and D. F. Kelley, *J. Chem. Phys.*, 1998, **108**, 9137–9143.

11. E. Dulkeith, T. Niedereichholz, T. Klar, J. Feldmann, G. von Plessen, D. Gittins, K. Mayya, and F. Caruso, *Phys. Rev. B*, 2004, **70**, 205424–1–205424–4.

12. M. B. Mohamed, V. Volkov, S. Link, and M. A. El-sayed, 2000, 517–523.

13. G. Ramakrishna, O. Varnavski, J. Kim, D. Lee, and T. Goodson, *J. Am. Chem. Soc.*, 2008, **130**, 5032–3.

14. M. Loumaigne, A. Richard, J. Laverdant, D. Nutarelli, and A. Débarre, *Nano Lett.*, 2010, **10**, 2817–2824.

15. M. Yorulmaz, S. Khatua, P. Zijlstra, A. Gaiduk, and M. Orrit, *Nano Lett.*, 2012, **12**, 4385–4391.

16. A. Tcherniak, S. Dominguez-Medina, W.-S. Chang, P. Swanglap, L. S. Slaughter, C. F. Landes, and S. Link, *J. Phys. Chem. C*, 2011, **115**, 15938–15949.

17. F. Wackenhut, A. V. Failla, and A. J. Meixner, *J. Phys. Chem. C*, 2013, **117**, 17870–17877.

18. M. Loumaigne, P. Vasanthakumar, A. Lombardi, A. Richard, and A. Débarre, *Phys. Chem. Chem. Phys.*, 2013, **15**, 4154–62.

19. M. Loumaigne and A. Débarre, in *SPIE Photonics Europe*, eds. D. L. Andrews, J.-M. Nunzi, and A. Ostendorf, International Society for Optics and Photonics, 2010, p. 77121V–77121V–10.

20. M. Loumaigne, P. Vasanthakumar, A. Richard, and A. Débarre, *ACS Nano*, 2012, **6**, 10512–23.

21. K. Goda and B. Jalali, *Nature Photon.*, 2013, **7**, 102–112.

22. J. R. G. Navarro, D. Manchon, F. Lerouge, N. P. Blanchard, S. Marotte, Y. Leverrier, J. Marvel, F. Chaput, G. Micouin, A.-M. Gabudean, A. Mosset, E. Cottancin, P. L. Baldeck, K. Kamada, and S. Parola, *Nanotechnology*, 2012, **23**, 465602.

23. J. R. G. Navarro, A. Liotta, A.-C. Faure, F. Lerouge, F. Chaput, G. Micouin, P. L. Baldeck, and S. Parola, *Langmuir*, 2013, **29**, 10915–21.

24. J. Burgin, M. Liu, and P. Guyot-Sionnest, *J. Phys. Chem. C*, 2008, **112**, 19279–19282.

25. E. C. Le Ru, J. Grand, I. Sow, W. R. C. Somerville, P. G. Etchegoin, M. Treguer-Delapierre, G. Charron, N. Félidj, G. Lévi, and J. Aubard, *Nano Lett.*, 2011, **11**, 5013–9.

26. A. Lombardi, M. Loumaigne, A. Crut, P. Maioli, N. Del Fatti, F. Vallée, M. Spuch-Calvar, J. Burgin, J. Majimel, and M. Tréguer-Delapierre, *Langmuir*, 2012, **28**, 9027–33.

27. E. S. Allgeyer, A. Pongan, M. Browne, and M. D. Mason, *Nano Lett.*, 2009, **9**, 3816–3819.

28. C. Hrelescu, T. K. Sau, A. L. Rogach, J. Frank, G. Laurent, L. Douillard, and F. Charra, *Nano Lett.*, 2011, **11**, 402–407.

29. S. Barbosa, A. Agrawal, L. Rodríguez-Lorenzo, I. Pastoriza-Santos, R. a Alvarez-Puebla, A. Kornowski, H. Weller, and L. M. Liz-Marzán, *Langmuir*, 2010, **26**, 14943–50.

30. R. Rodríguez-Oliveros and J. A. Sánchez-Gil, *Opt. Express*, 2012, **20**, 621.

31. F. Hao, C. L. Nehl, J. H. Hafner, and P. Nordlander, *Nano Lett.*, 2007, **7**, 729–32.

32. J. R. G. Navarro, F. Lerouge, G. Micouin, C. Cepraga, A. Favier, M. T. Charreyre, N. P. Blanchard, J. Lermé, F. Chaput, M. Focsan, K. Kamada, P. L. Baldeck, and S. Parola, *Nanoscale*, 2014, **6**, 5138–45.

33. J. R. G. Navarro, D. Manchon, F. Lerouge, E. Cottancin, J. Lermé, C. Bonnet, F. Chaput, A. Mosset, M. Pellarin, and S. Parola, *Nanotechnology*, 2012, **23**, 145707.

34. J. R. G. Navarro and M. H. V. Werts, *Analyst*, 2013, **138**, 583–92.

35. G. Deželić and J. P. Kratohvil, *Kolloid-Zeitschrift*, 1960, **173**, 38–48.

36. O. Varnavski, T. Goodson, M. Mohamed, and M. El-Sayed, *Phys. Rev. B*, 2005, **72**, 235405.

37. M. M. Tirado, C. L. Martínez, and J. G. de la Torre, *J. Chem. Phys.*, 1984, **81**, 2047–2052.

38. R. Rigler, Ü. Mets, J. Widengren, and P. Kask, *Eur. Biophys. J.*, 1993, **22**, 169–175.

39. S. W. Prescott and P. Mulvaney, *J. Appl. Phys.*, 2006, **99**, 1–8.